nature energy

ARTICLES

PUBLISHED: 8 AUGUST 2016 | ARTICLE NUMBER: 16113 | DOI: 10.1038/NENERGY.2016.113

Scalable synthesis of silicon-nanolayer-embedded graphite for high-energy lithium-ion batteries

Minseong Ko[1], Sujong Chae[1], Jiyoung Ma[1], Namhyung Kim[1], Hyun-Wook Lee[1,2]*, Yi Cui[2,3]* and Jaephil Cho[1]*

Existing anode technologies are approaching their limits, and silicon is recognized as a potential alternative due to its high specific capacity and abundance. However, to date the commercial use of silicon has not satisfied electrode calendering with limited binder content comparable to commercial graphite anodes for high energy density. Here we demonstrate the feasibility of a next-generation hybrid anode using silicon-nanolayer-embedded graphite/carbon. This architecture allows compatibility between silicon and natural graphite and addresses the issues of severe side reactions caused by structural failure of crumbled graphite dust and uncombined residue of silicon particles by conventional mechanical milling. This structure shows a high first-cycle Coulombic efficiency (92%) and a rapid increase of the Coulombic efficiency to 99.5% after only 6 cycles with a capacity retention of 96% after 100 cycles, with an industrial electrode density of $>1.6\,g\,cm^{-3}$, areal capacity loading of $>3.3\,mAh\,cm^{-2}$, and <4 wt% binding materials in a slurry. As a result, a full cell using $LiCoO_2$ has demonstrated a higher energy density ($1{,}043\,Wh\,l^{-1}$) than with standard commercial graphite electrodes.

Lithium-ion batteries (LIBs) are recognized as the most important power supply for mobile electronic devices, with energy densities that have been increasing by 7–10% per year[1,2]. There is a continuing demand for advanced LIBs with reduced weight, longer life spans, and higher capacity. However, conventional carbonaceous anodes are approaching their theoretical capacity limits[3–6]. In this regard, Si (ref. 7) and silicon oxide (SiO_x; ref. 8) have been considered as feasible alternatives for the next generation of LIB anodes. Their working potentials are low compared with graphite of <0.5 V versus Li/Li^+ (ref. 9). However, Si, which has a high theoretical specific capacity of $3{,}572\,mAh\,g^{-1}$ ($Li_{15}Si_4$) (ref. 10), generally induces extreme volume changes (>300%)[11], resulting in disintegration of the electrode during repeated charge/discharge processes[12,13]. To use Si as a negative electrode against volume expansion and control solid-electrolyte interphase (SEI) formation for high Coulombic efficiency (CE), advanced nanomaterial design strategies as an academic approach have been demonstrated, such as making double-walled Si nanotubes[14], Si–C yolk–shell and pomegranate structures[15–17], or graphene-encapsulated Si particles[18,19], suggesting a significant improvement in cycle life with relatively low areal mass loading for industrial implementation. Considering the practical standard, SiO_x has captured the interest of the industry due to its relatively low volume expansion (<200%), fewer side reactions with electrolytes, and high capacity retention on electrochemical cycling[20,21]. Nevertheless, since the included oxygen content of SiO_x can produce fatal irreversible products such as Li_2O and Li_4SiO_4 (refs 22,23), exploring the optimum stoichiometry of SiO_x and graphite-blended systems has presented formidable challenges[24,25]. Recently, it was reported that the optimal stoichiometry was $SiO_{1.06}$, but that the CE at the first cycle was as low as 75%[23]. Blending 3 wt% of $SiO_{1.06}$ with graphite achieved a reversible specific capacity of $397\,mAh\,g^{-1}$ with 76% capacity retention after 200 cycles in a full-cell system. However, this blending system suffers from SiO_x content limitation under 4 wt% because excessive use leads to a large increase of irreversible capacity losses in Li-confined full-cell systems.

Alternatively, Si-containing graphite composites have emerged with impressive potential for practical application in high-energy LIBs[26–30]. For example, refs 26,29 reported Si/graphite/C composites produced by a conventional ball-milling process with reversible specific capacities of 568 and $655\,mAh\,g^{-1}$, respectively. These two experiments achieved a CE of 86% at the first cycle, and ref. 29 reported a capacity retention of 71.4% after 300 cycles. However, these composites suffer from critical incompatibility between the irregular particle sizes of Si and graphite, even with excessive use of pitch as carbon glue, resulting in limited electrochemical performances. To accomplish a higher first-cycle CE >90%, lower side reactions with the electrolyte, and minimized volume expansion of the electrode, the following critical issues of current Si-containing graphite composites still remain: the homogeneous distribution of Si particles on the graphite surface; retaining particle uniformity for Si particle sizes less than tens of nanometre; optimization of the ratio between Si and graphite materials; and the graphite demolition problem by mechanical milling methods.

In this work, we have prepared Si-nanolayer-embedded graphite/carbon hybrids (SGC) using a chemical vapour deposition (CVD) process with a scalable furnace. This design has been demonstrated to produce 5 kg per batch using a small amount of silane gas (SiH_4), and has accomplished successful uniform distribution of Si nanolayers on graphite powder as shown in Fig. 1a,b (see the details of SiH_4 use for the raw materials in Supplementary Note 1). As a result, we have achieved enhanced reversible capacity ($517\,mAh\,g^{-1}$) with high CE (92%) at the first cycle. In addition, with the outstanding capacity retention, this hybrid effectively has overcome the electrode expansion problem even in the high electrode density case ($>1.6\,g\,cm^{-3}$) and areal

[1]Department of Energy Engineering, School of Energy and Chemical Engineering, Ulsan National Institute of Science and Technology (UNIST), Ulsan 44919, Republic of Korea. [2]Department of Materials Science and Engineering, Stanford University, Stanford, California 94305, USA. [3]Stanford Institute for Materials and Energy Sciences, SLAC National Accelerator Laboratory, Menlo Park, California 94025, USA. *e-mail: hyunwooklee@unist.ac.kr; yicui@stanford.edu; jpcho@unist.ac.kr

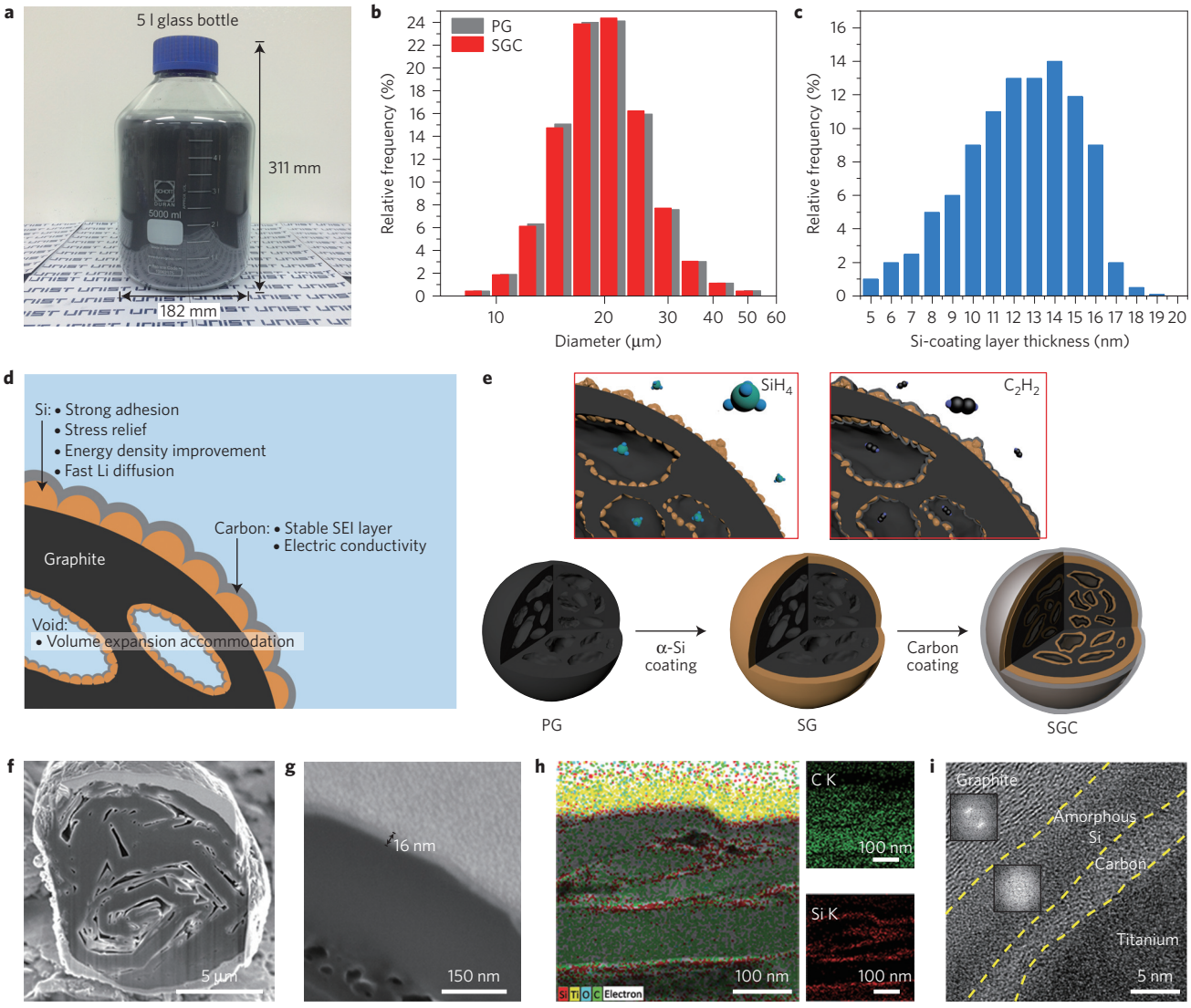

Figure 1 | Schematic of fabrication and characterization of the SGC hybrid. a, Photograph of the final product (5 kg) of SGC hybrids per batch. **b**, Statistical analysis of PG and SGC diameter variation before (grey) and after the CVD process (red). **c**, The overall thickness distribution of Si-coating layers on the graphite. **d**, Cross-sectional schematic view showing the detailed structural characteristics of a SGC hybrid particle. **e**, Schematic of the fabrication process for the SGC hybrid. Gas phase of SiH_4 and C_2H_2 can easily adsorb and penetrate on a pristine graphite (PG) surface and beneath its inner pores, which leads to homogeneous silicon and carbon coating. **f**,**g**, SEM images of cross-sectional SGC hybrids (**f**) and silicon nanolayer (**g**) on the graphite surface. **h**, STEM images for elemental mapping by energy-dispersive spectroscopy. **i**, High-resolution TEM image at the interfacial region of the SGC hybrid, with fast Fourier transform inset images. The yellow dotted curves indicate the boundaries between graphite, amorphous Si and carbon.

capacity loading of $>3.3\,mAh\,cm^{-2}$. All of these objectives were achieved using the conventional graphite anode process, which consists of an aqueous slurry composition with water-soluble SBR–CMC binder (<4 wt%).

Fabrication and characterization of SGC hybrid

The statistical analysis in Fig. 1b confirmed that the particle size distributions between pristine graphite (PG) and SGC hybrids were quite similar to each other (detailed images in Supplementary Fig. 1), and that the overall thickness of Si layers remained uniform even when quite thin (<20 nm) and flush on the graphite surface. For more details, Fig. 1c schematically shows the cross-section of a SGC hybrid to explain the structural characteristics. The Si nanolayer, both on the graphite particle and beneath its inner pores, led to a significant improvement of energy density. In addition, the nanosized characteristics[31] of the Si layer not only relieve the induced stress, but also allow fast diffusivity and high reactivity for Li-ion transport. The subsequent C coating provides high electric and ionic conductivity[32], and promotes more stable SEI formation[33] relative to pristine Si from electrolyte contact. Figure 1d illustrates the synthesis procedure for SGC hybrids. Interestingly, this unique gas decomposition process induces the facile penetration of the Si precursor into the empty volume space of the graphite, and also on the surface of graphite as a result of the uniform distribution of the Si nanolayer, followed by carbon coating following the same principles using C precursor (details are given in the Methods).

To verify its structural and compositional features, the SGC hybrid was examined by diverse analytical tools. Scanning electron microscope (SEM) images (see Supplementary Fig. 2) show the morphologies of the PG, the Si-nanolayer-embedded graphite (SG), and as-prepared SGC hybrids, clarifying their surface texture changes. Supplementary Fig. 2a corresponds to the smooth and even surface of PG with an average particle size of 18 μm, a high tap density of $1.0\,g\,cm^{-3}$, and a low specific surface area of

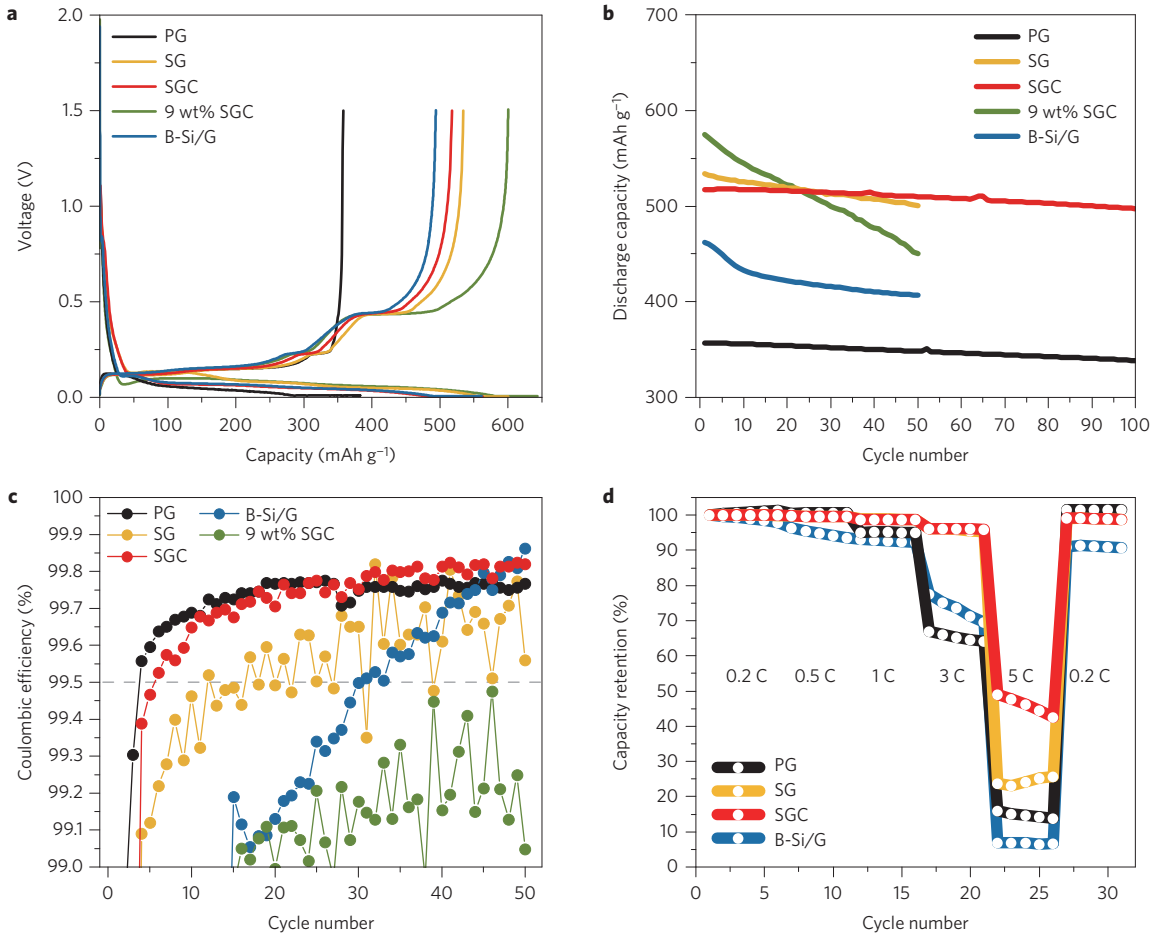

Figure 2 | Electrochemical characterization of various electrodes. a, Galvanostatic charge/discharge voltage profiles of PG, SG, SGC and B-Si/G measured at 0.1 C. **b**, Reversible discharge capacity versus cycle plot of PG, SG, SGC, 9 wt%-SGC, and B-Si/G cycled at 0.5 C for 100 cycles. **c**, Magnified form of stabilized efficiency for five different samples at each cycle to show how fast the CE reaches 99.5% from the first formation cycle. **d**, Rate capabilities of SGC under increasing C-rates from 0.2 C to 5 C, compared with PG, SG and B-Si/G.

5.2 $m^2 g^{-1}$. This type of spherical-shaped graphite is commercially and widely used as an anode, with a higher specific reversible capacity (~360 mAh g^{-1}) and CE (≥90%) than flake graphite[34].

The magnified image (Supplementary Fig. 2b) shows ultrafine Si nanoparticles with sizes of 5–20 nm homogeneously spread onto the surface of graphite. Through the thermal decomposition of acetylene gas (C_2H_2), SGC hybrids formed as a smooth carbon layer (<3 wt%) on the outermost surface of the Si layer as shown in Supplementary Fig. 2c. This carbon coating can suppress electrolyte decomposition and also provide enhanced electrochemical performance with facile electron transport in the electrode[31–33].

To confirm the chemical composition inside the SGC hybrid, a focused ion beam workstation was used to examine the interface composition between the Si layer and the spherical graphite powder by cross-sectional field-emission SEM and energy-dispersive spectroscopy mapping analysis in Fig. 1e–h. The sample was coated with Ti to protect its morphology while Ga^+ ions were induced[26]. The cross-sectional image shows that the spherical graphite particle contains many internal pores (Fig. 1e), and the uniform Si-coating layers were located beneath the pores inside and as well as on the outer surface of the graphite. The thickness of the outer shell was measured as ~16 nm (Fig. 1f). The Si-layer deposition beneath the pores was clearly identified via an elemental mapping image as shown in Fig. 1g. In addition, these Si layers adhere well onto the graphite surface in contrast to previous works[26–29,31,35], suggesting good electrical contact with the graphite. The interfaces between both the graphite and the Si layers, and the Si layers and the carbon coating, do not possess any voids, impurities, or secondary phases, as shown in the high-resolution transmission electron microscopy (TEM) image in Fig. 1h. Therefore, we note that the CVD process can lead to effective cell performance and carbon coating can prevent undesirable SEI formation on cycling, which results in a high CE of >90% at the first cycle and retention of a long cycle life.

Electrochemical testing of SGC hybrid

The synthesized SGC hybrid anode (including 6 wt% of Si content, and <3 wt% of C), PG, SG, physically blended nano-Si/graphite (B-Si/G), and 9 wt%-SGC (SGC hybrid containing 9 wt% Si and <3 wt% of C) were characterized using the constant current–constant voltage technique, with the results shown in Fig. 2. As shown in Fig. 2a, PG achieved a first-cycle gravimetric reversible capacity of 357 mAh g^{-1} with a very high CE of 92%. Interestingly, the SGC hybrid exhibits an identical CE of 92%, with an improved reversible specific capacity of 517 mAh g^{-1}. However, the B-Si/G anode recorded a relatively lower reversible capacity (494 mAh g^{-1}) and first-cycle CE (88%) because the crystalline Si nanopowders, as expected, led to undesirable powder heterogeneity with poor CE in a blended electrode, because of vastly different particle sizes and powder densities between the micrometre-sized graphite and nanosized Si (ref. 36). Moreover, the SG hybrid demonstrated higher specific reversible capacity (534 mAh g^{-1}) and lower CE (90%) than

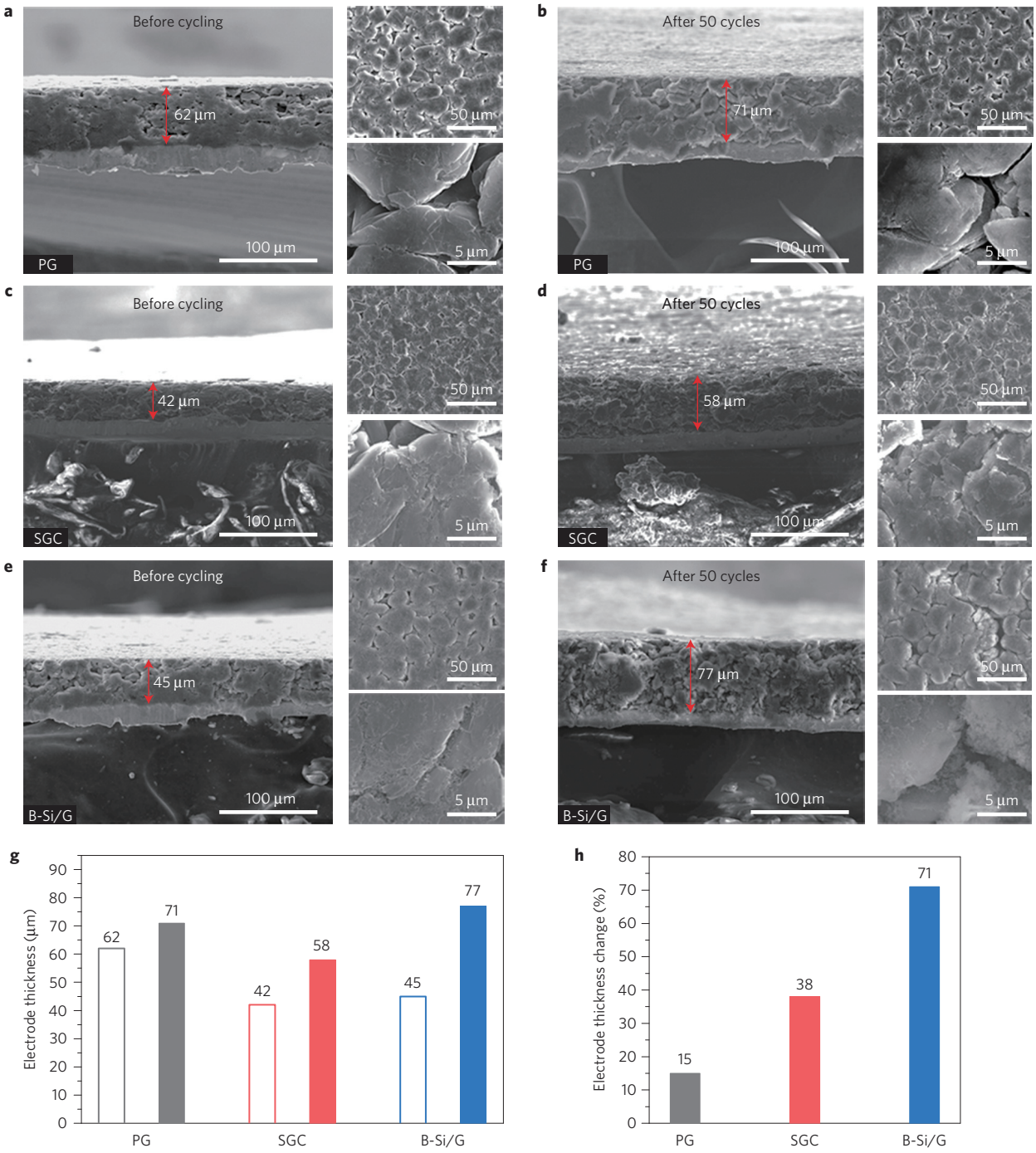

Figure 3 | Series of SEM images for electrode changes before and after 50 cycles. a–f, Cross-sectional view of PG, SGC, B-Si/G electrodes before cycling (**a**,**c**,**e**) and after 50 cycles (**b**,**d**,**f**), respectively. Top views of these electrodes are also shown at the right-hand side, with two resolution scales. The electrode composed of B-Si/G after 50 cycles (**f**) shows cracks on its surface as a result of large volume expansion, indicated by the arrows on the image. **g**,**h**, Charting the electrodes' thickness variation before cycling (open bars) and after 50 cycles (filled bars) (**g**), and the corresponding percentage change in electrode thickness (**h**).

that of the SGC hybrid. We believe that these properties are due to the presence of a carbon coating apparently playing a beneficial role for first-cycle CE enhancement, and a decrease of reversible specific capacity related to the carbon coating content (<3 wt%). In Fig. 2b, the SGC hybrid clearly shows improved cyclic stability with 96% capacity retention, confirming its comparability with PG (more extended cycling performance in Supplementary Fig. 3). However, when the Si-coating amounts were increased to 9 wt%, even the reversible specific capacity increased up to 596 mAh g^{-1}, but the excessively formed Si layer was not able to sustain its electrode interconnectivity, which strongly accelerated capacity fading after the first few cycles. Nevertheless, when the Si nanolayer coating was applied to carbon-coated graphite, the content of Si in SGC hybrids could also be improved showing better cyclic stability than 9 wt% SGC hybrid due to the mechanical carbon buffer matrix on the graphite (see the additional data in Supplementary Figs 4–6). Therefore, we believe that our Si-nanolayer-embedding process improved the capacity of a cell with stable cycle retention.

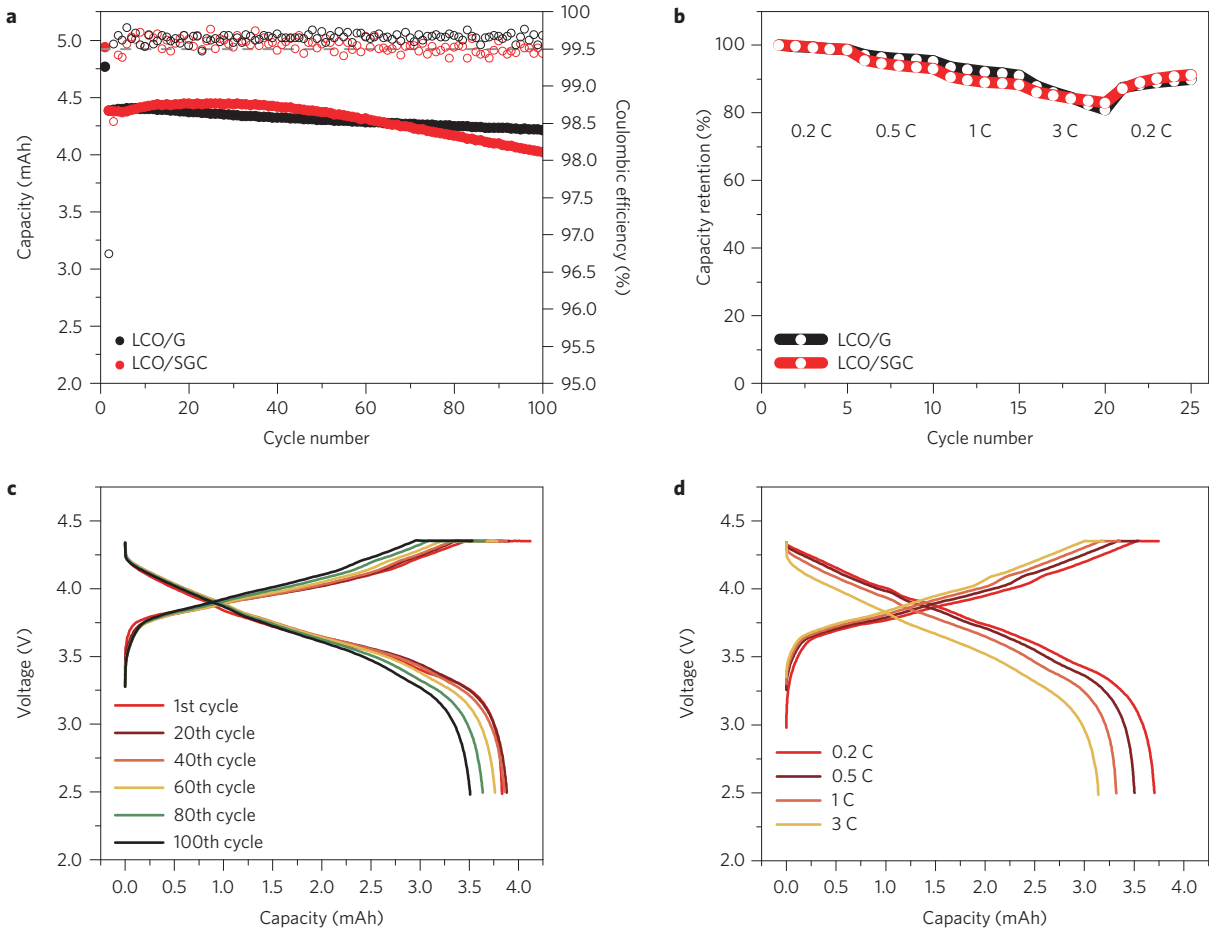

Figure 4 | Electrochemical comparison of a full cell between graphite (G) and SGC hybrid. a, Galvanostatic discharge capacities for 100 cycles at a discharge rate of 1 C with a constant charge rate of 0.5 C in the potential range from 2.5 V to 4.35 V. **b**, Capacity retention at various discharge rates from 0.2 C to 3 C. **c**,**d**, Voltage profiles for the LCO/SGC plotted as a function of the number of cycles (**c**) and as a function of the C-rate (**d**), respectively.

In Fig. 2c, we proved that the hybrids demonstrate a rapid increase of stabilized efficiency greater than 99.5% after only 6 cycles including the first formation cycle, and after 30 cycles it surpasses that of graphite. This enhanced CE higher than that of the PG results from the post-treated carbon coating process that decreases the specific surface area. For instance, as compared between PG and carbon-coated graphite as shown in Supplementary Fig. 7 and Supplementary Table 1, the reduced specific area of the carbon-coated graphite of 3.23 $m^2 g^{-1}$ leads to a better CE of 99.8% at only 4 cycles benefiting from less area of lithium consumption, such as the formation of SEI layers. For a long time, this cycling efficiency has been a decisive factor for commercialization of alloy anodes into full-cell systems, and thus our result is quite promising and has never been reported before. However, the SG, B-Si/G and 9 wt%-SGC anodes could not approach 99.5% stabilized efficiency even after a dozen cycles. Furthermore, the rate performance was measured by changing the discharge rates from 0.2 C to 5 C as shown in Fig. 2d. Owing to the high reactivity and diffusivity of nanoscaled Si for Li reaction combined with carbon coating effects[30], the SGC hybrid demonstrated the highest power capability and the highest current density in comparison with the other electrode anodes.

Volume expansion testing of fabricated electrodes

To observe the electrode thickness change and its surface morphology variation before and after 50 cycles, three different types of electrode (PG, SGC hybrid, and B-Si/G) were prepared with the same cell capacity, and investigated by SEM, and then by charting the electrodes thickness variation (Fig. 3). As shown in Fig. 3a,b, the electrode composed of PG clearly reveals a 15% thickness increase after 50 cycles with no signature of damage in the electrode or the particles, including no inter-particle cleavage, and demonstrates no electrical contact loss and capacity fading. The SGC electrode (Fig. 3c,d) exhibited a 38% thickness increase after 50 cycles and retained an electrode integrity comparable to that of PG. The volume expansion of about 40% can be accommodated on the industrial cell with the elaborate battery design (Supplementary Fig. 8). The SGC hybrids survived an additional 23% thickness variation whilst preserving the interconnectivity between the electrode composition materials. Thus, it allows volume expansion without any cracks on its surface by sustaining its pristine powder morphology after long-term cycling. However, the electrode composed of B-Si/G (Fig. 3e,f) underwent a thickness variation of 71% accompanied with severe cracks on its surface and loss of electrical contact between the electrode components[26], leading to drastic capacity loss and the formation of an unstable SEI layer. Therefore, the SGC electrode clearly preserves its electrical network, and entirely overcomes the detrimental effects of volume changes at industrial electrode composition levels. Figure 3g,h shows the charts of the thickness variations of all the electrodes before and after 50 cycles.

Electrochemical full-cell testing

A prototype full-cell device was built to demonstrate the commercial viability extension of a high-energy-density lithium-ion battery

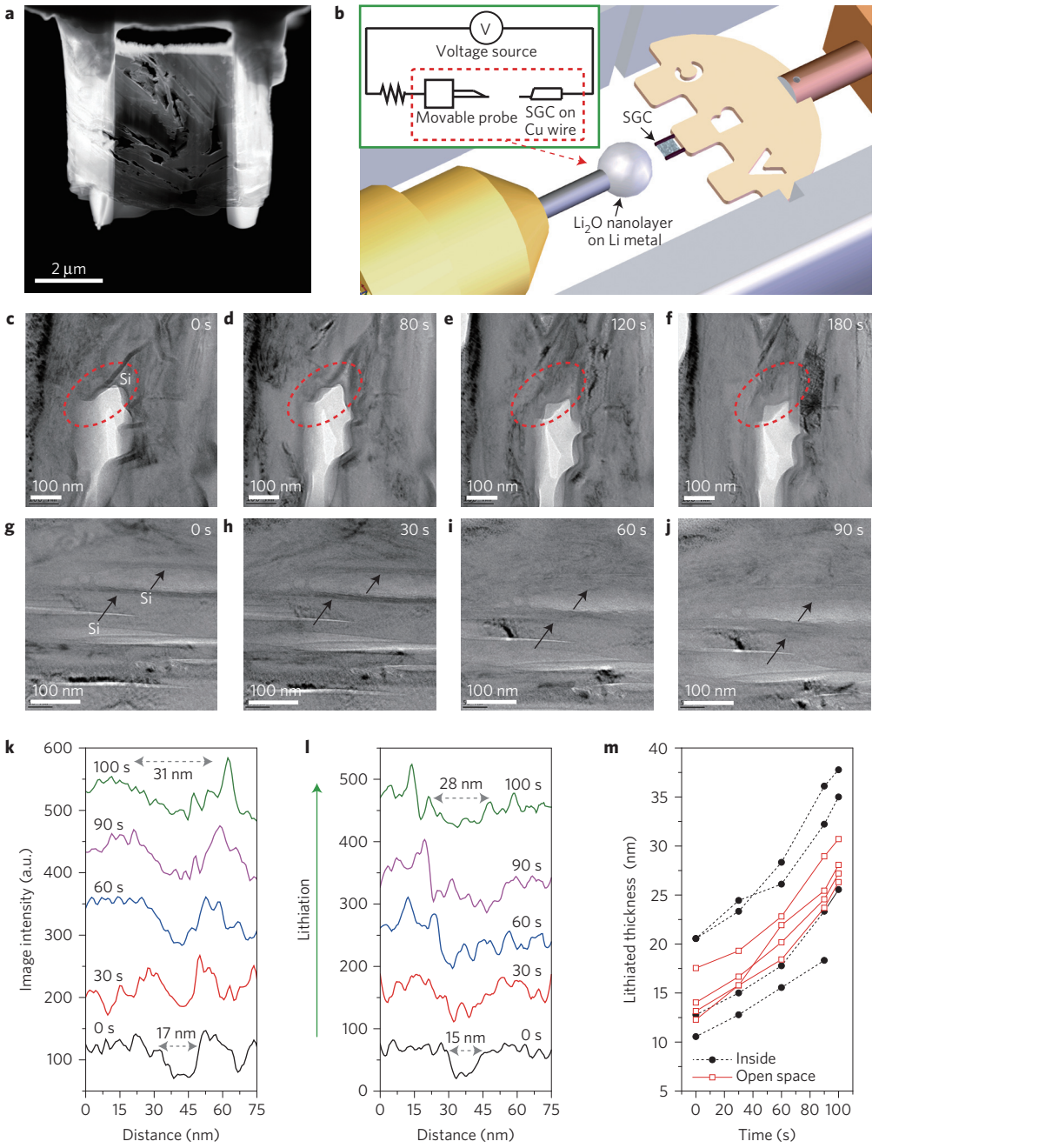

Figure 5 | ***In situ*** **TEM characterization of the SGC hybrid during lithiation. a**, Cross-sectional STEM image of SGC hybrid for *in situ* TEM test. **b**, Schematic illustrations of the electrochemical set-up for *in situ* TEM test and its circuit (inset). **c–j**, Captured *in situ* TEM images from time-lapse videos at two different regions of the hybrid, with time labels at the top right corner of the images. **c–f** show the behaviour of the silicon nanolayer (indicated by red ovals) coated on the surface of empty volume space during lithiation (Supplementary Video 1). **g–j** show the silicon nanolayer (indicated by arrows) located in the gap between graphite layers during lithiation (Supplementary Video 2). **k**,**l**, Line scans of the image intensity from **c–f** (**k**) and **g–j** (**l**) show the thickness of the expanded Si nanolayer during lithiation. **m**, The lithiated thickness variation with time.

system comprising a high-voltage lithium cobalt oxide (LCO) cathode and the SGC hybrid anode. The SGC/LCO full cell was compared with a commercial graphite anode full cell in the coin cell configuration over the potential range from 2.5 V to 4.35 V at 24 °C (Fig. 4). The fabricated SGC/LCO full-cell device demonstrated 92% capacity retention after 100 cycles, and an energy density of 1,043 $Wh\,l^{-1}$ with an average voltage of ~3.77 V (Fig. 4a) (detailed electrode information and energy density calculations are given in the Methods and Supplementary Note 2 and Supplementary Table 2). In addition, the stabilized efficiency exhibited a rapid increase upwards of 99.5% over only 6 cycles including the first cycle, at a discharge rate of 1 C. The graphite/LCO had 96% capacity retention with stabilized efficiency over only 3 cycles, and a relatively low energy density of 900 $Wh\,l^{-1}$ at an average voltage of ~3.87 V. Therefore, the SGC hybrid anode shows great potential for next-generation battery applications. In addition, capacity retention tests at various discharge rates from 0.2 to 3 C were carried out (Fig. 4b) following the capacity normalization. The measured values are comparable to those of the graphite/LCO cell because the rate capability is

limited by the high areal capacity loading (3.1 mAh cm^{-2}) of the lithium cobalt oxide (LCO) cathode. Figure 4c,d plots the voltage profiles of the SGC and LCO full cells for the above cycle and rate tests, respectively.

Discussion

According to our previous research, the mechanical interaction between lithiated particles possessing high volume expansion affects the kinetics of lithiation behaviour due to the increase of the Gibbs free energy[37]. The compressive stresses at the contact point between a lithiated Si nanopillar and a rigid wall increase rapidly, resulting in a change of the favoured lithiation orientation of ⟨110⟩ directions. The question of how the deposited Si nanolayer on graphite can effectively lithiate against mechanical interaction should also be considered to understand the effective lithiation of Si in the case of the SGC hybrid. We performed an *in situ* transmission electron microscopy investigation of the SGC hybrid anode to gain a fundamental understanding. The size of the standard SGC sample was too large for TEM, and so we fabricated a TEM sample using a focused ion beam as shown in the cross-sectional scanning TEM (STEM) image and schemes (Fig. 5a,b and see also Supplementary Fig. 9). A time series of the lithiation of Si nanolayers at two different positions is presented in Fig. 5c–f (deposited on void space) and Fig. 5g–j (between graphite layers), respectively (See also Supplementary Videos 1 and 2). To understand the lithiation behaviour of both cases, we plotted the lithiated thickness as a function of time during lithiation for a number of different layers (Fig. 5k–m). In both cases, the lithiated thickness increases approximately linearly with time, as shown in Fig. 5m, which suggested that the kinetics of the linear expansion is controlled by short-range interactions at an interface[38,39]. There will be mechanical stress caused by the interaction between Li_xSi and graphite, and consideration should be given as to how the lithiation behaviour of Si nanolayers between graphite layers can expand with the same kinetics. Since the deformation of Li_xSi starts earlier than that of graphite due to the higher electrochemical potential, the normal stress of Li_xSi pushes toward graphite layers during lithiation. The yield strength of Li_xSi is 1 GPa and the compressive strength of graphite is 55 MPa (refs 40,41), and thus the compressive strength of graphite is relatively negligible, which benefits lithiation of Si with less mechanical interaction from the adjunct graphite layers. Thus, it is found that graphite layers support effective lithium transport along the carbon matrix and do not block the expansion of Si, enabling remarkable battery performance.

We have therefore demonstrated that scalable optimum SGC hybrids successfully achieved higher volumetric energy density (1,043 Wh l^{-1}) than current commercial LIBs (900 Wh l^{-1}), and exhibited a Coulombic efficiency of 92% at the first cycle. Moreover, even with industrial electrode densities (>1.6 g cm^{-3}), and areal capacity loading of >3.3 mAh cm^{-2}, the fabricated SGC electrode demonstrated a rapid increase of cycling efficiency upward of 99.5% over only 6 cycles, in addition to favourable cyclability and high rate capability comparable to the industrial graphite anode. The electrode composed of SGC hybrids also completely overcame the detrimental effects arising from volume variation, and exhibited an additional expansion of only 23% compared with its graphite counterpart. This, in turn, completely preserved the electrical interconnectivity and morphological integrity without any cracks and contact losses. Moreover, a prototype full-cell device was demonstrated with a high-voltage lithium cobalt oxide cathode in a coin cell configuration, which achieved 92% capacity retention after 100 cycles. Consequently, this successful SGC hybrid anode has clear commercial viability for the next generation of high-energy battery systems, and could be a major breakthrough for electric vehicle or grid energy storage applications.

Methods

Preparation of SGC hybrid. The fabrication of SGC hybrid starts from spherical natural graphite. The spherical graphite was loaded into a rotatable furnace. To obtain homogeneous deposition of pure amorphous silicon on each graphite powder, high-purity silane gas (99.9999%) was streamed at a low flow rate of 1.5 l min^{-1} for 37 min per batch for 1 kg. Carbon coating was carried out with high-purity acetylene (C_2H_2) gas in the same furnace with a flow rate of 1.5 l min^{-1} for 8 min at 900 °C.

Material characterization. Structural investigation of the SGC hybrids was carried out using scanning electron microscopy (Verios 460, FEI) with energy-dispersive spectroscopy (Bruker XFlash 6130), high-resolution transmission electron microscopy (JEM-2100F, JEOL), and X-ray diffraction (D/MAZX 2500V/PC, Rigaku). Sample preparation for TEM analysis and cross-section view was carried out using a dual-beam focused ion beam (Helios 450HP, FEI). To observe the variations in electrode thickness and surface morphology after cycling, the cells are disassembled and the electrodes are rinsed with dimethyl carbonate in an argon-filled glove box.

***In situ* TEM analysis.** The *in situ* electrochemical characterization was carried out in an FEI Titan 80-300 environmental TEM at the acceleration voltage of 300 kV. A Nanofactory Instruments Dual-Probe STM-TEM *in situ* sample holder was employed to demonstrate the lithiation behaviour on the Si/graphite composites. During transfer of the Li metal counter electrode inside the TEM, the Li metal was exposed to air for about 5 s to create a thin Li_2O layer of about 20 nm functioning as a solid electrolyte. A relative bias of −3.5 V was applied between the two electrodes, which caused Li^+ ions to be transferred to the Si/graphite electrode through the solid electrolyte. During the observation, the electron beam was spread out to avoid beam effects.

Electrochemical characterization. Working electrodes were made by casting slurry on a Cu current collector with active material (SGC hybrid, PG, SG, SGC containing 9 wt% Si, and B-Si/G), sodium carboxymethyl cellulose (CMC), styrene butadiene rubber (SBR), and carbon black (Super P, TIMCAL) at a mass ratio of 95.8:1.7:1.5:1; the loading level of homogeneously blended slurry with SGC was ∼6.5 mg cm^{-2}, and the case of graphite was ∼9.5 mg cm^{-2}, respectively. All electrodes were dried at 80 °C for 2 h, and then pressed until the density of the electrode became >1.6 g cm^{-3} with the electrode thickness of 42 μm of the SGC electrode and 62 μm of the PG electrode except for the Cu current collector, and finally vacuum-dried at 110 °C overnight. 2032 coin-type cells were assembled in an argon-filled glove box containing pure Li metal foil (1 mm) as the counter electrode. The electrolyte was 1.3 M $LiPF_6$ in ethylene carbonate/diethyl carbonate (3:7 vol%; Panax Starlyte) with 10% fluoroethylene carbonate (Panax Starlyte) and microporous polyethylene was used as a separator with a thickness of 20 μm. 2032-R coin-type cells were assembled in a glove box filled with argon gas. Electrochemical properties of the half-cell were evaluated under the voltage window between 0.005 and 1.5 V for the first and second cycles, and between 0.005 and 1.0 V for the rest of the cycles. All electrochemical tests were carried out using a TOSCAT-3100 battery cycler (TOYO SYSTEM).

The full cell was designed with a N/P ratio of ∼1.1; the cathode and anode areal capacities were 3.1 mAh cm^{-2} and 3.3 mAh cm^{-2}, respectively. The cathode electrode was fabricated by casting slurry on a Al current collector with commercialized lithium cobalt oxide (LCO), carbon black, and polyvinylidene fluoride (PvdF) binder in the weight ratio of 94:3:3; the loading level of slurry with LCO was ∼19 mg cm^{-2}. The electrodes were dried at 110 °C for 1 h, and then pressed until the density of the electrode became >3.5 g cm^{-3} with the electrode thickness of 51 μm excepting for the Al current collector. *N*-methyl-2-pyrrolidone (NMP) was used as the solvent. 2032-R coin-type cells were assembled in a glove box filled with argon gas. The electrolytes and separator in the full cell were the same as those in the half-cell above. Electrochemical analysis of the full cell was carried out in the voltage window between 2.5 and 4.35 V. All electrochemical tests were done using a TOSCAT-3100 battery cycler (TOYO SYSTEM).

Received 25 February 2016; accepted 7 July 2016; published 8 August 2016

References

1. Jeong, G., Kim, Y.-U., Kim, H., Kim, Y.-J. & Sohn, H.-J. Prospective materials and applications for Li secondary batteries. *Energy Environ. Sci.* **4**, 1986–2002 (2011).
2. Crabtree, G., Kócs, E. & Trahey, L. The energy-storage frontier: lithium-ion batteries and beyond. *MRS Bull.* **40**, 1067–1078 (2015).
3. Choi, N. S. *et al.* Challenges facing lithium batteries and electrical double-layer capacitors. *Angew. Chem. Int. Ed.* **51**, 9994–10024 (2012).

4. Thackeray, M. M., Wolverton, C. & Isaacs, E. D. Electrical energy storage for transportation—approaching the limits of, and going beyond, lithium-ion batteries. *Energy Environ. Sci.* **5**, 7854–7863 (2012).
5. Goodenough, J. B. Evolution of strategies for modern rechargeable batteries. *Acc. Chem. Res.* **46**, 1053–1061 (2013).
6. Rolison, D. R. & Nazar, L. F. Electrochemical energy storage to power the 21st century. *MRS Bull.* **36**, 486–493 (2011).
7. Zhang, W. J. A review of the electrochemical performance of alloy anodes for lithium-ion batteries. *J. Power Sources* **196**, 13–24 (2011).
8. Obrovac, M. N. & Chevrier, V. L. Alloy negative electrodes for Li-ion batteries. *Chem. Rev.* **114**, 11444–11502 (2014).
9. Nitta, N. & Yushin, G. High-capacity anode materials for lithium-ion batteries: choice of elements and structures for active particles. *Part. Part. Syst. Charact.* **31**, 317–336 (2014).
10. Obrovac, M. N. & Christensen, L. Structural changes in silicon anodes during lithium insertion/extraction. *Electrochem. Solid-State Lett.* **7**, A93–A96 (2004).
11. Mcdowell, M. T., Lee, S. W., Nix, W. D. & Cui, Y. 25th anniversary article: understanding the lithiation of silicon and other alloying anodes for lithium-ion batteries. *Adv. Mater.* **25**, 4966–4985 (2013).
12. Ko, M., Oh, P., Chae, S., Cho, W. & Cho, J. Considering critical factors of Li-rich cathode and Si anode materials for practical Li-ion cell applications. *Small* **11**, 4058–4073 (2015).
13. Wu, H. & Cui, Y. Designing nanostructured Si anodes for high energy lithium ion batteries. *Nano Today* **7**, 414–429 (2012).
14. Wu, H. *et al.* Stable cycling of double-walled silicon nanotube battery anodes through solid-electrolyte interphase control. *Nature Nanotech.* **7**, 309–314 (2012).
15. Liu, N. *et al.* A yolk-shell design for stabilized and scalable Li-ion battery alloy anodes. *Nano Lett.* **12**, 3315–3321 (2012).
16. Lu, Z. *et al.* Nonfilling carbon coating of porous silicon micrometer-sized particles for high-performance lithium battery anodes. *ACS Nano* **9**, 2540–2547 (2015).
17. Liu, N. *et al.* A pomegranate-inspired nanoscale design for large-volume-change lithium battery anodes. *Nature Nanotech.* **9**, 187–192 (2014).
18. Luo, J. *et al.* Crumpled graphene-encapsulated Si nanoparticles for lithium ion battery anodes. *J. Phys. Chem. Lett.* **3**, 1824–1829 (2012).
19. Li, Y. *et al.* Growth of conformal graphene cages on micrometre-sized silicon particles as stable battery anodes. *Nature Energy* **1**, 15029 (2016).
20. Lee, J.-I. & Park, S. High-performance porous silicon monoxide anodes synthesized via metal-assisted chemical etching. *Nano Energy* **2**, 146–152 (2013).
21. Song, J.-W., Nguyen, C. C. & Song, S.-W. Stabilized cycling performance of silicon oxide anode in ionic liquid electrolyte for rechargeable lithium batteries. *RSC Adv.* **2**, 2003–2009 (2012).
22. Miyachi, M., Yamamoto, H., Kawai, H., Ohta, T. & Shirakata, M. Analysis of SiO anodes for lithium-ion batteries. *J. Electrochem. Soc.* **152**, A2089–A2091 (2005).
23. Suh, S. S. *et al.* Electrochemical behavior of SiO_x anodes with variation of oxygen ratio for Li-ion batteries. *Electrochim. Acta* **148**, 111–117 (2014).
24. Dimov, N., Xia, Y. & Yoshio, M. Practical silicon-based composite anodes for lithium-ion batteries: fundamental and technological features. *J. Power Sources* **171**, 886–893 (2007).
25. Du, Z., Dunlap, R. A. & Obrovac, M. N. High energy density calendered Si alloy/graphite anodes. *J. Electrochem. Soc.* **161**, A1698–A1705 (2014).
26. Jo, Y. N. *et al.* Si–graphite composites as anode materials for lithium secondary batteries. *J. Power Sources* **195**, 6031–6036 (2010).
27. Lee, J.-H., Kim, W.-J., Kim, J.-Y., Lim, S.-H. & Lee, S.-M. Spherical silicon/graphite/carbon composites as anode material for lithium-ion batteries. *J. Power Sources* **176**, 353–358 (2008).
28. Li, M. *et al.* Facile spray-drying/pyrolysis synthesis of core–shell structure graphite/silicon-porous carbon composite as a superior anode for Li-ion batteries. *J. Power Sources* **248**, 721–728 (2014).
29. Yoon, Y. S., Jee, S. H., Lee, S. H. & Nam, S. C. Nano Si-coated graphite composite anode synthesized by semi-mass production ball milling for lithium secondary batteries. *Surf. Coat. Technol.* **206**, 553–558 (2011).
30. Alias, M. *et al.* Silicon/graphite nanocomposite electrode prepared by low pressure chemical vapor deposition. *J. Power Sources* **174**, 900–904 (2007).
31. Kasavajjula, U., Wang, C. S. & Appleby, A. J. Nano- and bulk-silicon-based insertion anodes for lithium-ion secondary cells. *J. Power Sources* **163**, 1003–1039 (2007).
32. Saint, J. *et al.* Towards a fundamental understanding of the improved electrochemical performance of silicon-carbon composites. *Adv. Funct. Mater.* **17**, 1765–1774 (2007).
33. Yoshio, M. *et al.* Carbon-coated Si as a lithium-ion battery anode material. *J. Electrochem. Soc.* **149**, A1598–A1603 (2002).
34. Yoshio, M. *et al.* Improvement of natural graphite as a lithium-ion battery anode material, from raw flake to carbon-coated sphere. *J. Mater. Chem.* **14**, 1754–1758 (2004).
35. Uono, H., Kim, B.-C., Fuse, T., Ue, M. & Yamaki, J.-I. Optimized structure of silicon/carbon/graphite composites as an anode material for Li-ion batteries. *J. Electrochem. Soc.* **153**, A1708–A1713 (2006).
36. Lee, E. H. *et al.* Effect of carbon matrix on electrochemical performance of Si/C composites for use in anodes of lithium secondary batteries. *Bull. Korean Chem. Soc.* **34**, 1435–1440 (2013).
37. Lee, S. W. *et al.* Kinetics and fracture resistance of lithiated silicon nanopillar pairs controlled by their mechanical interaction. *Nature Commun.* **6**, 7533 (2015).
38. Liu, X. H. *et al.* Ultrafast electrochemical lithiation of individual Si nanowire anodes. *Nano Lett.* **11**, 2251–2258 (2011).
39. Mcdowell, M. T. *et al. In situ* TEM of two-phase lithiation of amorphous silicon nanospheres. *Nano Lett.* **13**, 758–764 (2013).
40. Sethuraman, V. A., Chon, M. J., Shimshak, M., Srinivasan, V. & Guduru, P. R. *In situ* measurements of stress evolution in silicon thin films during electrochemical lithiation and delithiation. *J. Power Sources* **195**, 5062–5066 (2010).
41. Boylan, J. Smooth operators: carbon-graphite materials. *Mater. World* **4**, 707–708 (1996).

Acknowledgements

This work was supported by the IT R&D programme of the Ministry of Trade, Industry & Energy/Korea Evaluation Institute of Industrial Technology (MOTIE/KEIT) (Development of Li-rich Cathode and Carbon-free Anode Materials for High Capacity/High Rate Lithium Secondary Batteries, 10046306) and the 2016 Research Fund (1.160033.01) of UNIST (Ulsan National Institute of Science and Technology). Also, Y.C. acknowledges support from the Assistant Secretary for Energy Efficiency and Renewable Energy, Office of Vehicle Technologies, Battery Materials Research Program of the US Department of Energy.

Author contributions

M.K. conceived and designed the experiments, and performed data interpretation. M.K. prepared the samples and carried out the main experiments. S.C. assisted with the data interpretation and designed the experimental scheme; H.-W.L. conducted *in situ* TEM characterization and detailed discussion on analytic results. J.M. assisted with sample preparation and performed the energy-dispersive spectroscopy measurement. N.K. provided data analysis. M.K., S.C., H.-W.L., Y.C. and J.C. co-wrote the paper.

Additional information

Supplementary information is available online. Reprints and permissions information is available online at www.nature.com/reprints. Correspondence and requests for materials should be addressed to H.-W.L., Y.C. or J.C.

Competing interests

The authors declare no competing financial interests.